NANO · MICRO small
www.small-journal.com

Triblock Proteins with Weakly Dimerizing Terminal Blocks and an Intrinsically Disordered Region for Rational Design of Condensate Properties

*Dmitrii Fedorov, Nelmary Roas-Escalona, Dmitry Tolmachev, Adam L. Harmat, Alberto Scacchi, Maria Sammalkorpi, A. Sesilja Aranko, and Markus B. Linder**

Condensates are molecular assemblies that are formed through liquid–liquid phase separation and play important roles in many biological processes. The rational design of condensate formation and their properties is central to applications, such as biosynthetic materials, synthetic biology, and for understanding cell biology. Protein engineering is used to make a triblock structure with varying terminal blocks of folded proteins on both sides of an intrinsically disordered mid-region. Dissociation constants are determined in the range of micromolar to millimolar for a set of proteins suitable for use as terminal blocks. Varying the weak dimerization of terminal blocks leads to an adjustable tendency for condensate formation while keeping the intrinsically disordered region constant. The dissociation constants of the terminal domains correlate directly with the tendency to undergo liquid–liquid phase separation. Differences in physical properties, such as diffusion rate are not directly correlated with the strength of dimerization but can be understood from the properties and interplay of the constituent blocks. The work demonstrates the importance of weak interactions in condensate formation and shows a principle for protein design that will help in fabricating functional condensates in a predictable and rational way.

1. Introduction

Liquid–liquid phase separation (LLPS) is widespread in biology.[1,2] In LLPS, typically a protein- or RNA/DNA- containing liquid, spontaneously separates into a dense and dilute phase.[3] The dense phase is observed as liquid-like droplets. The droplets are often called condensates or coacervates, with the former prevailing in the context of cell biology.[4,5] For synthetic biology, for probing cellular biology, and biological materials engineering, it is central that we have tools and understanding for a rational design of condensates.[6,7]

LLPS is an intermediate step in the assembly of biological materials such as has been described for in squid beaks,[8] mollusk adhesives and shells,[9,10] and for protein fiber formation.[11,12] Condensates function as intermediate states that can undergo further changes into amyloids, gels, fibers, or aggregates.[8,12–14] In cells— particularly in eukaryotic ones— LLPS plays an important role by forming membrane-less organelles that have roles in, for example, RNA processing, stress response, and development.[15–19]

A key feature of LLPS is that the configurational entropy of participating polymers decreases—order increases—within the dense phase.[20] For materials formation, LLPS is therefore interesting because condensates form an intermediate stage toward the final structure. It follows that many engineered molecular structures that undergo LLPS are attracting much interest for new bioengineered materials, food technology, drug delivery, and analytical techniques.[21–26]

D. Fedorov, N. Roas-Escalona, M. Sammalkorpi, A. S. Aranko, M. B. Linder
Department of Bioproducts and Biosystems
Aalto University
P.O. Box 16100, Aalto FI-00076, Finland
E-mail: markus.linder@aalto.fi

The ORCID identification number(s) for the author(s) of this article can be found under https://doi.org/10.1002/smll.202306817

DOI: 10.1002/smll.202306817

D. Fedorov, N. Roas-Escalona, D. Tolmachev, A. L. Harmat, A. Scacchi, M. Sammalkorpi, A. S. Aranko, M. B. Linder
Center of Excellence in Life-Inspired Hybrid Materials (LIBER)
Aalto University
P.O. Box 16100, Aalto FI-00076, Finland

D. Tolmachev, A. L. Harmat, A. Scacchi, M. Sammalkorpi
Department of Chemistry and Materials Science
Aalto University
P.O. Box 16100, Aalto FI-00076, Finland

A. Scacchi
Department of Applied Physics
Aalto University
P.O. Box 11000, Aalto FI-00076, Finland

In synthetic biology and for molecularly engineered biological materials it is important to be able to structurally design condensates for specific properties.[6] Therefore, much effort has been put into engineering macromolecular features and interactions involved. Intrinsically disordered regions (IDRs) in proteins have been widely found to affect LLPS. IDRs are highly repetitive, flexible, and lack a defined 3D structure. Their amino acid composition can vary widely, giving rise to a range of interactions involving charge, π-stacking, hydrogen bonding, and hydrophobicity.[27–30] LLPS is therefore sensitive to conditions such as temperature, pH, and salt screening.[31,32] The individual interactions are weak, and are described in the terminology of polymer science as "sticker-interactions".[33] Properties depend on the cooperativity of these repetitive stickers. A successful approach to adjusting condensate properties has been to tune the strength of their IDR – interactions.[34] The overall architecture of proteins plays a large role. A commonly observed arrangement is that a flexible IDR sequence is linked to a folded protein like a tail. The chain length of IDRs affects properties.[35] Folded proteins can be oligomerizing, resulting in multivalent structures capable of cross-linking and cooperativity.[36] One strategy for condensate engineering involved the construction of multivalent architectures using interacting domains with high affinities ranging from 10^{-6} to 10^{-11} M.[37] Conditions for LLPS often involve high concentrations of cosolutes. The presence of other macromolecules affects condensate formation by, for example, competing weak interactions and crowding. Interfacial tensions of condensates are low—in the range of μNm^{-1}—but in many ways play an important role in the properties of condensates.

In this study, we explore how weak interactions between folded proteins in combination with IDRs can be used for rational molecular engineering of condensates. We experimentally explore design principles for the overall architecture of engineered proteins to undergo LLPS. We have noted that proteins undergoing LLPS and engineered versions of them are affected strongly by the presence of terminal domains that have individually folding structures.[38,39] We took the triblock architecture found in these proteins as a model and designed proteins with varying functionalities as terminal blocks (**Figure 1**). As the midblock, we used the IDR sequence from the ADF3 dragline silk of the spider *Araneus diadematus*.[40] In ADF3 the repeats contain stretches of on average six alanine residues flanked by longer stretches rich in glutamine. The alanine stretches form hydrophobic sticker- interactions between chains.[12] The ADF3 sequence contained 12 repeats and was kept the same in all variants. As terminal blocks, we chose functionally unrelated domains. These had similar folds and sizes and based on preliminary analyses could represent a range of different dimerization affinities, starting from ultra-weak to medium strength.

2. Results and Discussion

2.1. Protein Architecture

We engineered proteins with a triblock architecture consisting of an IDR-midblock which was capped at both termini by two globular proteins serving as terminal blocks (Figure 1a–c; Table S1, Supporting Information). The IDR-midblock was constant in all variants and consisted of a 542-amino acid long part of the native ADF3 spidroin. The globular terminal blocks were: A cellulose binding module from the *Clostridium thermocellum* cellulosome[41] (CBM), SpyCatcher002[42] (SC), human fibronectin III domain 10 [43] (FN), and human γD-crystallin[44] (Crys). The terminal blocks were also expressed as individual proteins to determine their properties. All four terminal block proteins have approximately the same size and are structurally similar (Figure S1, Supporting Information). All proteins were produced in *Escherichia coli* and purified by affinity chromatography.

2.2. Quantification of Dimerization for Terminal Blocks

We initially determined the strength of dimerization, that is, binding affinity, of the isolated terminal blocks using the dissociation constants (K_d) determined by analytical ultracentrifugation (AUC). We verified the K_d for CBM dimerization to be 90 μM as previously reported.[45] We performed sedimentation velocity experiments and collected the sedimentation profiles of SC, FN, and Crys at multiple protein concentrations. Initial analysis was performed by the van Holde–Weischet (vHW) method (Figure 1d). Both FN and Crys displayed a shift toward higher sedimentation coefficients with an increase in protein concentration. This shift of the distribution to a higher sedimentation coefficient together with the shape of the curves in turn represents the formation of oligomers. SC, however, did not display any signs of self-association even at a concentration of 0.5 mM.

We selected appropriate methods for data analysis based on the vHW analysis.[45] For SC we used the 2DSA method (Figure S2, Supporting Information). For FN, we used the C(s) method in combination with fitting a binding isotherm using weight-average sedimentation coefficients, giving a K_d of 2300 μM (Figure S3, Supporting Information). For Crys a K_d of 2.8 μM was calculated by a global fit of sedimentation equilibrium data (Figure S4, Supporting Information). Crys data were also analyzed by the ls*-g(s) method.[46] The range of K_d values for the terminal domains spans several orders of magnitude (**Table 1**).

2.3. Impact of Terminal Blocks on the Tendency of Triblock Proteins to Undergo LLPS

LLPS was determined by observing the formation of condensate droplets using a light microscope. We used the amount of crowding agent required for LLPS as a measure of the propensity to undergo condensation.[47,48] Condensation was observed also without crowding, but at higher protein concentrations. The crowding agent Dextran 500 was chosen since does not interact with silk proteins.[49] The solution contained 100 mM NaCl. Multiple combinations of dextran and protein at different concentrations were used to map the tendency of each variant to undergo LLPS (**Figure 2**).

The four proteins showed differences in their tendencies to undergo LLPS. Crys-ADF3-Crys had the strongest tendency and

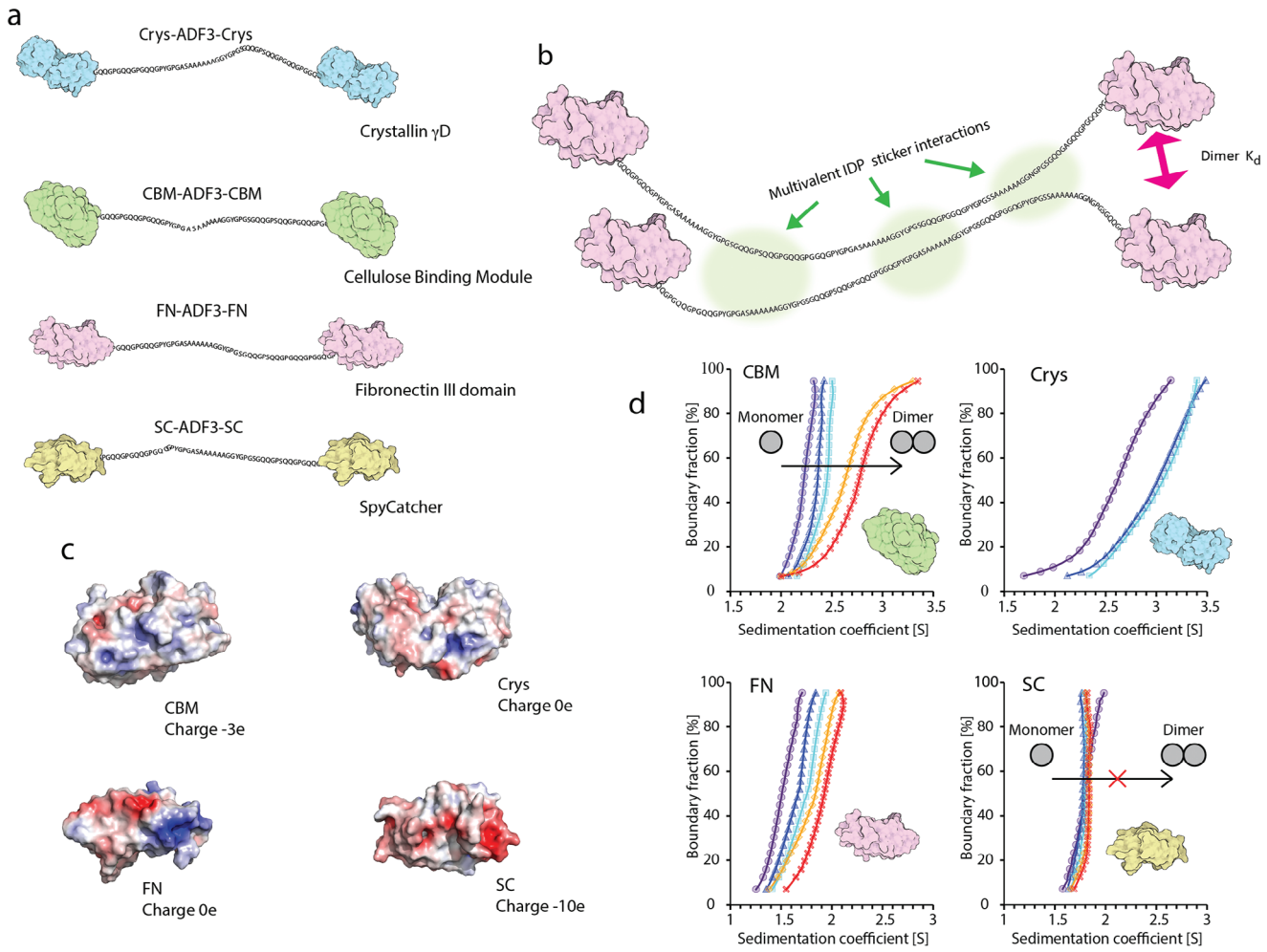

Figure 1. a) Schematic representation of the four variants of the ADF3 with different terminal blocks. Proteins and linkers are not drawn to scale. b) The silk IDR exhibits weak sticker interactions and the terminal blocks dimerization interactions. c) The terminal blocks are similar in size but differ in their surface charges. The range of electrostatic surface potential is shown from $-5k_BT/e$ (red color) to $+5k_BT/e$ (blue color). d) AUC data. Van Holde–Weischet distribution of the four terminal blocks at different protein concentrations: CBM in concentration range from 3 (violet circles) to 267 μM (red crosses); Crys: 0.4 μM – violet circles, 1 μM – blue triangles, and 2.4 μM – cyan squares; FN in concentration range from 126 μM (violet circles) to 2.3 mM (red crosses); SC from 7 μM (violet circles) to 450 μM (red crosses). The shifts in curve positions show that all proteins except SC show a concentration-dependent association.

underwent LLPS at dextran concentrations already 30 gL^{-1} across the whole studied protein concentration range. Microscope images of condensate droplets in the different regions are shown in Figure S5a–d (Supporting Information). The tendency became then weaker in the order, CBM-ADF3-CBM, FN-ADF3-FN, and SC-ADF3-SC (Figure 2e). The tendency to undergo LLPS correlated directly with the K_d values of the terminal domains. The protein and dextran concentration needed for LLPS increased in the order of decreasing terminal domain interactions. One interpretation of the results is that terminal domain

Table 1. Physical properties of the triblock protein variants and their condensates.

Protein	K_d of terminal block, [μM]	Diffusion coefficient, [$\mu m^2 s^{-1}$]	Inverse capillary velocity, [$s\mu m^{-1}$]	Surface tension, [$\mu N m^{-1}$]
SC-ADF3-SC	Not measurable[a)]	0.19 ± 0.02	0.0260 ± 0.0018	234 ± 84
FN-ADF3-FN	2300	1.01 ± 0.12	0.0038 ± 0.0011	284 ± 32
CBM-ADF3-CBM	90	0.27 ± 0.04	0.0072 ± 0.0016	213 ± 144
Crys-ADF3-Crys	2.8	0.51 ± 0.40	0.0053 ± 0.0011	162 ± 78

[a)] No dimers were detected even at the highest concentration of 0.5 mM.

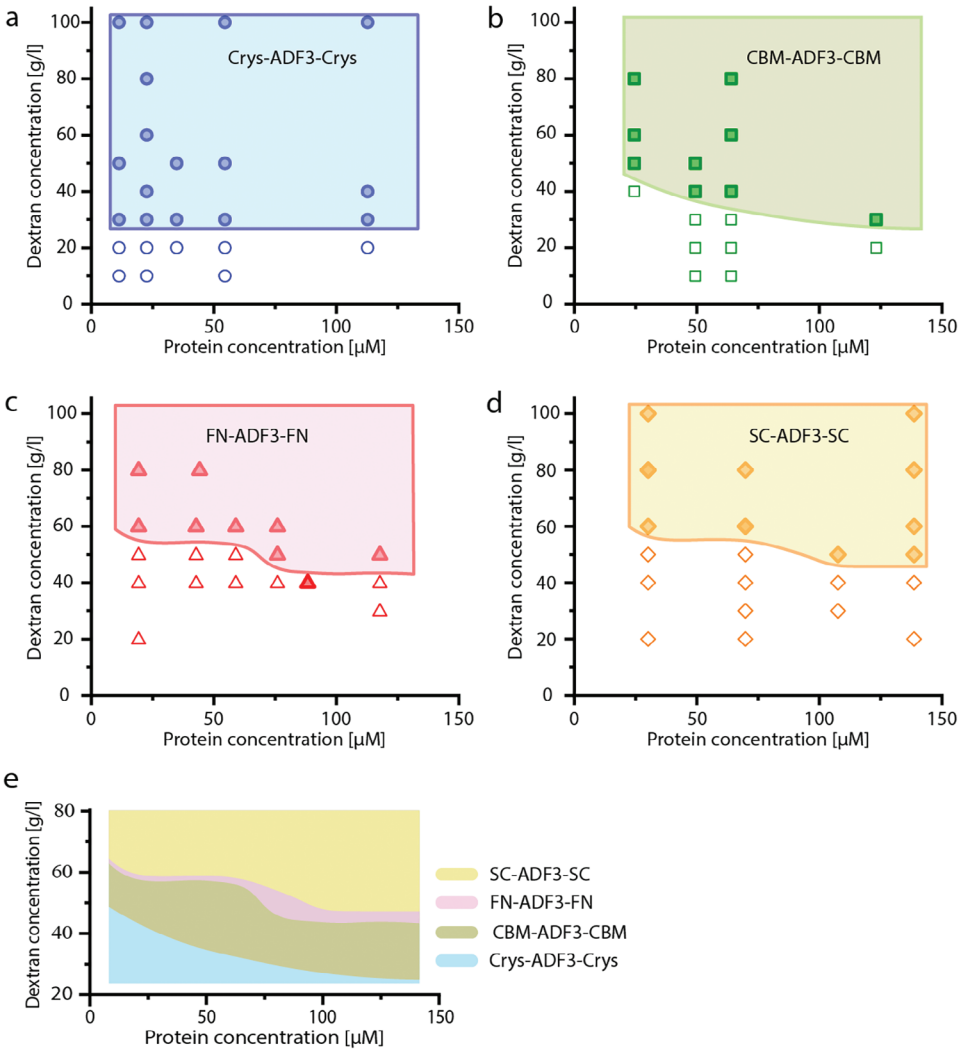

Figure 2. Mapping the tendency of the four terminal block variants to undergo LLPS. The lower the minimal concentration of dextran resulting in LLPS, the higher the propensity for LLPS. Open symbols indicate no LLPS, filled symbols show LLPS. Colored regions serve as a guideline – LLPS was observed inside the area and was not observed outside. a) Crys-ADF3-Crys — blue circles. b) CBM-ADF3-CBM — green squares. c) FN-ADF3-FN — red triangles. d) SC-ADF3-SC —orange diamonds. e) Overlap of phase diagrams highlights the ranking of the variants in terms of the tendency to undergo LLPS.

dimerization effectively increases the chain length of the protein, leading to a higher degree of entanglement and/or interactions.[34,35] A similar prediction has been made for systems of globular proteins.[50] Terminal domain dimerization can also enhance colocalization and therefore increase the weak sticker interactions of the IDR.[51] To qualitatively understand the argument, we can calculate the fraction of terminal domains that would be in dimer form at a particular concentration. Using for example a concentration of 100 μM which is in the mid-range of protein concentration used as shown in Figure 2 — we can calculate the fraction of proteins in dimer form: Crys 95%, CBM 50%, FN 4%, and SC 0%. Inside the condensates, the fraction of proteins in dimer form will be larger as concentrations are higher. These K_d-values in the range of millimolar to micromolar are therefore in a range relevant for condensation. If interactions were stronger, above that of Crys, the fraction of molecules in contact at 100 μM or higher would not increase markedly as the effect of increasing it further from 95% would not be very significant.

2.4. Differences in the Terminal Domains Affect the Physical Properties of the Condensates

To understand further correlations between terminal domains and LLPS, we continued to study the physical properties of the condensates. As a robust technique to probe both viscosity and surface tension, we determined inverse capillary velocities (ICV) for all variants (**Figure 3**a,b and Table 1). The ICV values were calculated from video recordings of condensate fusion events (Figure 3a). The value of ICV corresponds to the ratio of viscosity to surface tension (η/γ).[52] Low viscosity (η) and high surface tension (γ) lead to rapid droplet fusion (low slope) while high η and low γ lead to slow fusion (steep slope).

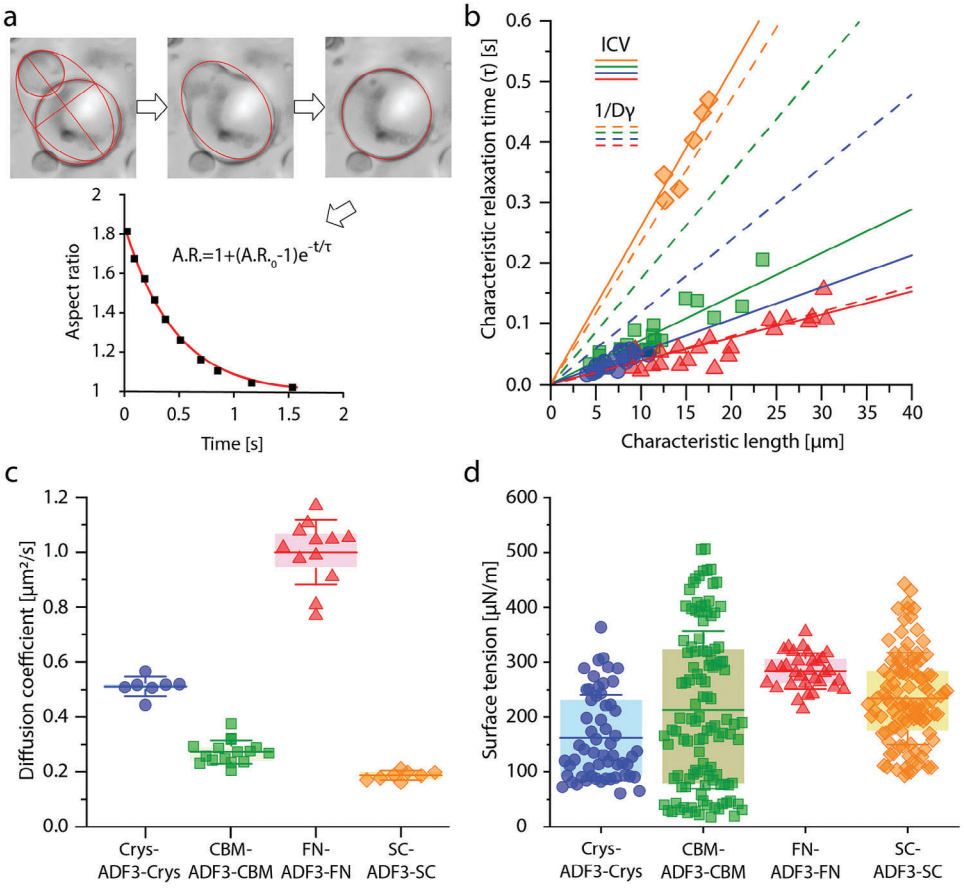

Figure 3. a) Data points for inverse capillary velocity (ICV) calculations were obtained by analyzing video recordings of droplet coalescence. b) The ICV values for the variants correspond to the slopes of the solid lines. The ratio $1/D\gamma$ obtained from independently measured values for the diffusion coefficient and surface tension data is shown as dashed lines. Symbols are explained in (c) and (d). c) Diffusion coefficients obtained from FRAP experiments. d) Surface tension values obtained by colloidal probe AFM measurements.

To better understand the results, we used fluorescence recovery after photobleaching (FRAP) to measure the diffusion of molecules inside the coacervates. Diffusion coefficients (D) were calculated based on the recovery profiles (Figure 3c, Table 1; Figure S6, Supporting Information). Diffusion coefficients were distinctly different between variants. FN-ADF3-FN was clearly the most rapidly diffusing while SC-ADF-SC was the slowest diffusing one. We used the technique of capillary bridging in colloidal probe AFM to measure the surface tension of the coacervate droplets (Figure 3d; Figure S7, Supporting Information).

Because diffusion is inversely proportional to viscosity based on the Stokes–Einstein equation[53] we approximated ICV by calculating $1/D\gamma$ using FRAP and AFM data (Figure 3b, dashed lines). The relative order of $1/D\gamma$ and ICV (η/γ) was the same by both methods, verifying independently the relative ranking in capillary velocities. The difference in absolute values can be expected in this approximation. First, the calculation of ICV includes some arbitrary choices in determining the a and b axis in the enclosing ellipse (Figure 3a) and the calculations do not consider the viscosity of the surrounding medium. Second, using the Stokes–Einstein equation for comparing protein variants we would also need to assume that the effective size of the protein would be the same—which they necessarily are not. It is interesting to note that the largest deviations in the comparison are for Crys-ADF3-Crys and CBM-ADF3-CBM which have the strongest dimerization propensity and therefore expected to have a comparably larger effective size. Not taking this into account would overestimate the slope in accordance with what is observed.

A clear correlation between K_d-values of terminal blocks and diffusion rate and surface tension is not observed. Elsewhere it has been widely described that the viscosity of dense protein solutions rises from the complex interplay of different factors, but it does show some general trends where attractions, repulsions, and geometry are important.[54–57] For FN-ADF3-FN and SC-ADF3-SC, their response to variations of salt gives some insight (**Figure 4**). The above experiments were performed in 100 mM NaCl in order to screen electrostatic interactions. The presence of salt and thereby screening of electrostatic interactions is required for reliable K_d-values by AUC since otherwise, the resulting nonidealities lead to inconclusive results.[58] The charge of SC is −10e, while FN has zero net charge, but it has a structure that forms a significant electric dipole (Figure 1c). We further tested salt-free conditions for LLPS and found that SC-ADF3-SC did not undergo LLPS at any of the protein concentrations tested, but with the added NaCl LLPS was achieved. Electrostatic repulsion between SC-blocks without salt and screening

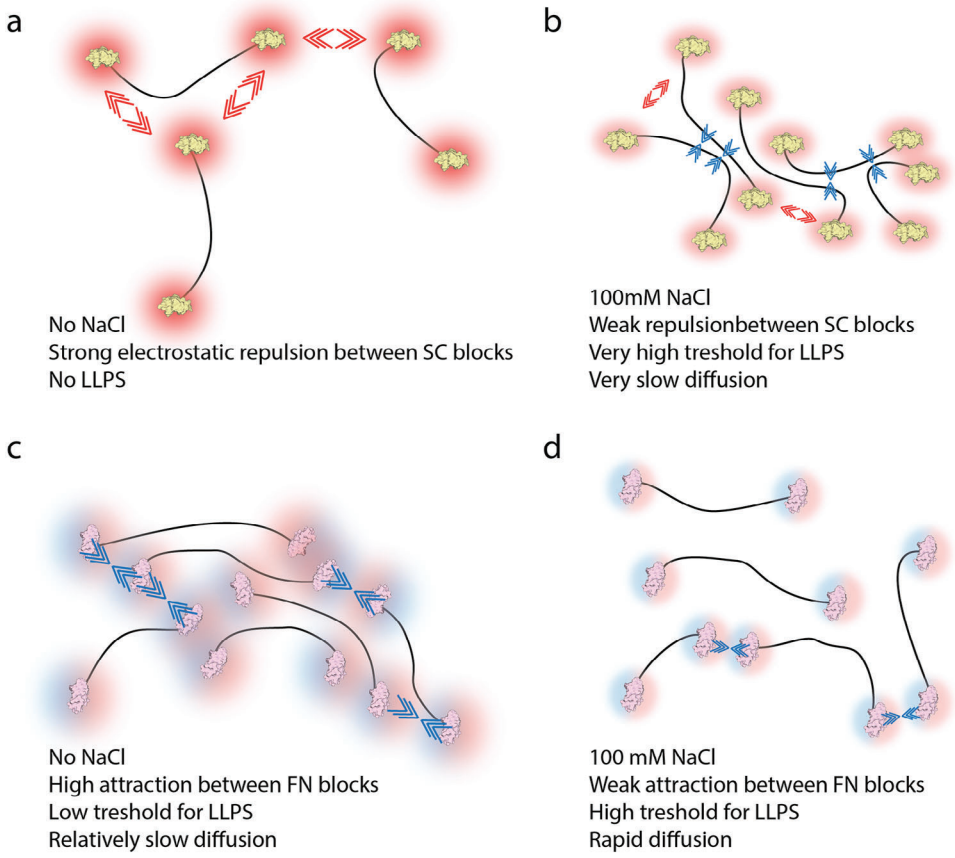

Figure 4. Schematic representation of how the presence of salt affects LLPS and molecular diffusion. Red arrows indicate repulsion and blue indicates attraction. a) In a salt-free solution SC-ADF3-SC did not undergo LLPS. The strong negative charge of SC can cause strong electrostatic repulsion. b) Adding 100 mM NaCl screens the electrostatic repulsion and leads to LLPS at high concentrations of the crowding agent. c) In a salt-free solution FN-ADF3-FN readily underwent LLPS at low concentrations of crowding agent. d) Adding 100 mM NaCl reduced the tendency of FN-ADF3-FN to undergo LLPS markedly. Since FN has a distinct dipolar charge distribution, the reduced tendency of LLPS can be understood by screening the dipolar charge interactions by NaCl.

of the repulsion with salt explains this behavior (Figure 4a,b).[59] The attractions between the mid-IDR block must therefore be driving the LLPS of SC-ADF3-SC. In general, the viscosity of protein solutions with internal repulsions coupled with attractive clustering is expected to be particularly high, as these conditions lead to reduced protein mobility.[60,61] SC-ADF3-SC at 100 mM NaCl represents such a condition (Figure 4b), since the negative charge of SC is still expected to result in internal repulsion, and the observed LLPS is mediated by the multivalent IDR-interactions of ADF3.

FN-ADF3-FN showed an opposite response to electrostatic screening by NaCl compared to SC-ADF3-SC. NaCl decreased the tendency of FN-ADF3-FN to undergo LLPS, compared to the non-screening (no NaCl) condition (Figure 4c,d; Figure S8, Supporting Information). If FN blocks interact by dipolar charge interactions, their interactions are expected to be stronger when electrostatics are not screened than if they are. This is what was observed. We measured the diffusivity of FN-ADF3-FN in salt-free conditions giving a value of 0.2 $\mu m^2\ s^{-1}$ (Figure S9, Supporting Information). This value is much lower than that at 100 mM NaCl ($\approx$1 $\mu m^2\ s^{-1}$). It has been shown that proteins forming coupled interactions have increased viscosity.[62] The increased dipolar interactions when charges are not screened are therefore expected to show lower diffusion compared to when the dipolar interactions are weaker with NaCl present. The particularly high diffusion of FN-ADF3-FN would therefore be a result of the relatively weak—but still attractive—terminal block interactions. The differences in diffusion observed here thus follow what is generally known for dense protein solutions. The absolute magnitudes are difficult to predict but electrostatic repulsions or attractions — as well as the anisotropy of these— are highly important, as are cluster formations and interactions leading to chain-like assemblies.[63] The involvement of both terminal block and IDR interactions makes this interplay between parts highly complex. The Crys and CBM variants did not show marked effects by changes between conditions when charges were screened or not. They showed low to intermediate diffusion values, agreeing with their rather strong terminal block affinities leading to the coupling between molecules.

3. Conclusion

The triblock approach keeping a constant IDR segment and weakly interacting terminal blocks in this study was driven by

the idea that LLPS is a key step toward biological materials formation.[12] Often the multiple weak sticker interactions of IDRs will be central for forming the materials properties. For example when the aim is to make materials such as adhesives or silks, where properties are based on specific features of the IDR regions.[11] In silk, the alanine stretches of IDRs are critical for functions as they show a subsequent switch from α-helices to β-sheets which play an important role for materials properties.[23] With this work, we propose that a triblock approach is a useful strategy to controllably tune condensation and the initial properties of condensates. As the properties of the IDR-containing condensates can be tuned, it allows for selecting assembly conditions, which can be used to design suitable technical processing conditions. This will allow for more feasible routes for biomimetic materials than available for the native molecule designs, as the native designs could require us to follow the natural—and technically unfeasible— biological conditions.

We found that dimerization constants (K_d) of terminal domains correlated logically with the propensity for condensation. Terminal domain affinity can bring colocalization which in turn can enable weak sticker interactions between IDRs.[51] However, alone the affinity of terminal domains alone is insufficient to predict the properties of condensates. For diffusion rates, we found that the nature of the interactions between terminal domains—especially if the interactions were electrostatic and their charge distribution[56]—strongly affect properties. Terminal domain characteristics can provide an opportunity to engineer diffusivity—and by extension viscosity—but effects can be difficult to predict because the underlying mechanisms are complex. However, a systematic approach in which well-characterized terminal domains are used could allow engineering a predictable behavior for condensates.

In particular, the conclusion of this work is the need to understand the nature of very weak interactions between proteins. Methods for studying and understanding weak interactions — such as AUC— will be important. A toolbox of weakly interacting protein terminal blocks could be further developed and explored together with IDRs for a rational approach toward engineered LLPS systems for diverse protein materials and wider use in biomolecular science.

4. Experimental Section

Recombinant Protein Expression: All constructs were cloned into pEt28-vectors as fusion proteins with His-tags to allow purification by affinity chromatography. Cloning of constructs coding for CBM, [12] CBM-ADF3-CBM, [12] and SC-ADF3-SC[35] had been reported before. To construct the plasmids coding for FN, Crys, SC, Crys-ADF3-Crys, and FN-ADF3-FN, the sequences coding for the terminal domains and the middle fragment were ordered as synthetic genes followed by assembly into pEt28-vectors to result in desired architectures. The protein sequences for all constructs are shown in Table S1 (Supporting Information). All proteins were recombinantly expressed using *E. coli* strain BL21 (DE3) (ThermoFisher Scientific) and MagicMedia (ThermoFisher Scientific) expression medium following the manufacturer's instruction. Cell lysis was performed with a high-pressure homogenizer EmulsiFlex. Protein purification was performed by immobilized metal affinity chromatography (IMAC). An ÄKTA-Pure liquid chromatography system (GE Healthcare Life Sciences) with a 5 mL His-Trap column was used for IMAC of the supernatant. Proteins were transferred into water or 100 mM NaCl for subsequent experiments by gel filtration. All proteins contain a 6xHis-tag in the C-terminus. The amino acid sequences are shown in Table S1 (Supporting Information).

Analytical Ultracentrifugation: Sedimentation experiments were conducted using a Beckman Coulter Optima analytical ultracentrifuge using the An-60 Ti rotor and standard 12 mm Epon centerpieces in all experiments. All measurements were performed at a temperature of 20 °C. Sedimentation velocity experiments were used to study both FN and SC. SC was measured in absorbance mode at the following concentrations and wavelengths: 7 μM at 280 nm and 75, 300, and 450 μM at 300 nm. The rotor speed was 60 000 RPM. FN was studied at 126 μM concentration in absorbance mode and in 436–2.34 mM concentration range in interference mode. The rotor speed in experiments with FN was 50 000 RPM. Data analysis was carried out by Sedfit and Ultrascan.[64,65] In the Crys sedimentation equilibrium experiments, measurements were performed at three rotor speeds: 27 000, 35 000, and 42 000 RPM with three loading concentrations: 0.5, 1, 2 μM. The experiments were made in absorbance mode at 230 nm. Data were analyzed by Sedphat.[66] GUSSI[67] visualization software was used for data obtained in Sedfit and Sedphat. Other details of experimental design and data analysis procedures were as published previously.[45]

Fluorescence Recovery After Photobleaching: FRAP imaging was performed using a Leica TSC SP5 confocal microscope and a 63 × 1.2 NA water objective as previously described.[49] An argon laser (488 nm) and a 488/561 dichroic beam splitter were used. The triblock proteins were labeled with Oregon Green 488 dye (ThermoFisher Scientific) according to the manufacturer's protocol. All samples were additionally flushed with MQ water using Vivaspin 6 centrifugal concentrator tubes to remove unbound dye molecules. Samples for FRAP were prepared by mixing dextran and protein to have a final concentration of a sample of 15 gL^{-1} protein and 10% dextran. Data treatment was made by LAS X software (Leica). Diffusion coefficients (D) were calculated in MatLab according to the Equation (1).[68]

$$I(t) = I_0 \cdot \left(1 - \sqrt{\frac{w^2}{w^2 + 4\pi Dt}}\right) \quad (1)$$

where $I(t)$ is intensity as a function of time, I_0 is the plateau intensity, w is the diameter of the bleached area, and t is the time after bleaching. CD spectroscopy is used to verify that the labeling reaction did not affect protein structures (Figure S10, Supporting Information).

LLPS Analysis: CBM-ADF3-CBM, SC-ADF3-SC, Crys-ADF3-Crys, and FN-ADF3-FN protein samples were mixed with dextran 500 at different concentrations in 100 mM NaCl or water. Both dextran and protein samples were diluted beforehand to provide a 1:1 dextran-to-protein ratio in the final mixture. A Zeiss Axio Vert A1 optical microscope was used to inspect the protein solution for condensate presence.

Inverse Capillary Velocity: Protein samples were mixed with dextran 500 in 100 mM NaCl buffer. The final concentration of dextran was 10%. The concentration of proteins was chosen to provide multiple and big enough coacervates. Microscope imaging was performed by Zeiss Axio Vert A1 inverted optical microscope. Events of droplets coalescence were recorded for further shape analysis. Shape analysis was performed essentially as previously described.[16] Fusing droplets were approximated by an ellipse where the long axis was the maximum distance between the borders of droplets. The short axis was calculated from the long axis and volume of an ellipse. The volume of the ellipse assumes that volume was constant during coalescence and equal to the sum of volumes of fusing droplets. Volumes of fusing droplets were calculated assuming that they were spheres. Radiuses of spheres and distances between droplets borders were directly obtained from ZEN microscope software. Graphs of aspect ratio versus time were approximated to determine characteristic relaxation time by Equation (2):

$$A.R.(t) = 1 + (A.R._0 - 1) \cdot e^{-\frac{t}{\tau}} \quad (2)$$

where $A.R. = \frac{l_{long}}{l_{short}}$ is the aspect ratio, l_{long} is the long axis of the ellipse, l_{short} is the short axis of the ellipse, $A.R._0$ is the aspect ratio right before coalescence, t is the time from the beginning of coalescence, and τ is the characteristic relaxation time.

Plots of characteristic relaxation time (τ) versus characteristic length (l) were fit to Equation (3):

$$\frac{\tau}{l} = \frac{\eta}{\gamma} \text{or } \tau = \frac{\eta}{\gamma} \cdot l \quad (3)$$

where, η is the viscosity, and γ is the surface tension. The characteristic length was calculated as a geometric mean $l = \sqrt{(l_{long,\,0} - l_{short,\,0}) \cdot l_{short,\,0}}$, where $l_{long,0}$ and $l_{short,0}$ – axis before coalescence. The fit determines the ICV $\frac{\eta}{\gamma}$. All fitting procedures were made using Origin software.

Surface Tension Measurements by AFM: The interfacial energy was determined using a colloidal probe atomic force microscopy (CP-AFM) from spectroscopy experiments. Solutions containing condensates were prepared by mixing 60 gL^{-1} of dextran, and 100 mM NaCl with 5–10 gL^{-1} of the triblock proteins. A glass sphere probe (CP-qp-CONT-BSG, D≈5 µm) was used to measure the asymmetric adhesion of coacervates, which prebound firmly to mica and bound temporarily to the AFM tip surface during measurement. The force curves were measured at a rate of 4 Hz and calibrated spring constant between 0.06 and 0.15 Nm^{-1}. JPKSPM data analysis software and Origin 2020 software (OriginLab Corporation) were used to analyze and process the force curves. The force curves were taken on coacervates with 20–30 repetitions at 10 s of contact time. This contact time was considered long enough to form the capillary bridge between the coacervate and the glass probe. The interfacial tension was calculated from capillary adhesion force at zero separation, which was valid close to saturation. The capillary forces measured in the CP-AFM setup for this system do not show signs of hysteresis. The hysteresis-free nature of the force–distance measurements allowed to use equilibrium thermodynamics to analyze the results. Then by following the method of Sprakel et al.,[69,70] when the capillary bridge was near its binodal concentration, meaning that saturation conditions apply, the attractive force, extrapolated to zero separation, follows the equation: $\lim_{\mu \to \mu*} F_{h=0} = -2\pi R\gamma \cos(\theta)$. Where R is the radius of the spherical probe, θ is the contact angle at the three-phase contact line. Then, the above extrapolation was carried out by plotting all the force curves simultaneously for each coacervate and using the region of attractive force to extrapolate linearly to zero separation, using MatLab. Data are presented as mean ± s.d. (standard deviation). The value of s.d. was obtained from the data of four condensate droplets × 25 force curves.

Supporting Information

Supporting Information is available from the Wiley Online Library or from the author.

Acknowledgements

The authors acknowledge the provision of facilities by the Bioeconomy Infrastructure and the RAMI—RawMatters Finland Infrastructure at Aalto University and the computational resources by the CSC IT Centre for Finland. MSc Yin Yin and MSc Ellinor Englund are thanked for their help with the cloning of recombinant proteins. This work was supported by the Academy of Finland through projects #317395 and #333238, the Center of Excellence Program (2022-2029) in Life-Inspired Hybrid Materials (LIBER) (projects #346105 and #346111), and the Novo Nordisk Foundation (#NNF20OC0061306, #NNF23OC0081564, and #NNF22OC0074060).

Conflict of Interest

The authors declare no conflict of interest.

Author Contributions

D.F. expressed and purified the proteins, did AUC experiments and analyzed the data, determined phase behavior, inverse capillary velocity, diffusivity, and drafted the first version of the manuscript. N.R. determined surface tensions. D.T., A.L.H., A.S., and M.S. helped in interpreting the data. A.S.A. was responsible for the recombinant DNA work. All authors participated in preparing the manuscript. M.B.L. supervised the work and finalized the manuscript.

Data Availability Statement

The data that support the findings of this study are available from the corresponding author upon reasonable request.

Keywords

biomaterials, coacervate, liquid–liquid phase separation, protein dimer, protein engineering

Received: August 9, 2023
Revised: October 20, 2023
Published online:

[1] S. Alberti, *Curr. Biol.* **2017**, *27*, R1097.
[2] J. Berry, C. P. Brangwynne, M. Haataja, *Rep. Prog. Phys.* **2018**, *81*, 046601.
[3] J. Wang, J.-M. Choi, A. S. Holehouse, H. O. Lee, X. Zhang, M. Jahnel, S. Maharana, R. Lemaitre, A. Pozniakovsky, D. Drechsel, I. Poser, R. V. Pappu, S. Alberti, A. A. Hyman, *Cell* **2018**, *174*, 688.
[4] A. A. Hyman, C. A. Weber, F. Jülicher, *Annu. Rev. Cell Dev. Biol.* **2014**, *30*, 39.
[5] S. Alberti, A. A. Hyman, *Nat. Rev. Mol. Cell Biol.* **2021**, *22*, 196.
[6] Y. Dai, L. You, A. Chilkoti, *Nat. Rev. Bioeng.* **2023**, s44222.
[7] Z.-G. Qian, S.-C. Huang, X.-X. Xia, *Nat. Chem. Biol.* **2022**, *18*, 1330.
[8] Y. Tan, S. Hoon, P. A. Guerette, W. Wei, A. Ghadban, C. Hao, A. Miserez, J. H. Waite, *Nat. Chem. Biol.* **2015**, *11*, 488.
[9] J. H. Waite, *J. Exp. Biol.* **2017**, *220*, 517.
[10] S. Y. Bahn, B. H. Jo, Y. S. Choi, H. J. Cha, *Sci. Adv.* **2017**, *3*, e1700765.
[11] A. Miserez, J. Yu, P. Mohammadi, *Chem. Rev.* **2023**, 2049.
[12] P. Mohammadi, A. S. Aranko, L. Lemetti, Z. Cenev, Q. Zhou, S. Virtanen, C. P. Landowski, M. Penttilä, W. J. Fischer, W. Wagermaier, M. B. Linder, *Commun. Biol.* **2018**, *1*, 86.
[13] M. C. Hardenberg, T. Sinnige, S. Casford, S. T. Dada, C. Poudel, E. A. Robinson, M. Fuxreiter, C. F. Kaminksi, G. S. Kaminski Schierle, E. A. A. Nollen, C. M. Dobson, M. Vendruscolo, *J. Mol. Cell Biol.* **2021**, *13*, 282.
[14] U. Rana, C. P. Brangwynne, A. Z. Panagiotopoulos, *J. Chem. Phys.* **2021**, *155*, 125101.
[15] C. P. Brangwynne, C. R. Eckmann, D. S. Courson, A. Rybarska, C. Hoege, J. Gharakhani, F. Jülicher, A. A. Hyman, *Science* **2009**, *324*, 1729.
[16] C. P. Brangwynne, T. J. Mitchison, A. A. Hyman, *Proc. Natl. Acad. Sci. USA* **2011**, *108*, 4334.
[17] P. Li, S. Banjade, H.-C. Cheng, S. Kim, B. Chen, L. Guo, M. Llaguno, J. V. Hollingsworth, D. S. King, S. F. Banani, P. S. Russo, Q.-X. Jiang, B. T. Nixon, M. K. Rosen, *Nature* **2012**, *483*, 336.
[18] N. Gilks, N. Kedersha, M. Ayodele, L. Shen, G. Stoecklin, L. M. Dember, P. Anderson, *Mol. Biol. Cell* **2004**, *15*, 5383.
[19] M. Fuxreiter, M. Vendruscolo, *Nat. Cell Biol.* **2021**, *23*, 587.
[20] Y.-H. Lin, J. D. Forman-Kay, H. S. Chan, *Biochemistry* **2018**, *57*, 2499.

[21] D. Zwicker, R. Seyboldt, C. A. Weber, A. A. Hyman, F. Jülicher, *Nat. Phys.* **2017**, *13*, 408.
[22] K. K. Nakashima, M. H. I. Van Haren, A. A. M. André, I. Robu, E. Spruijt, *Nat. Commun.* **2021**, *12*.
[23] P. Mohammadi, A. S. Aranko, C. P. Landowski, O. Ikkala, K. Jaudzems, W. Wagermaier, M. B. Linder, *Sci. Adv.* **2019**, *5*, eaaw2541.
[24] N. Chen, Z. Zhao, Y. Wang, R. Dimova, *ACS Macro Lett.* **2020**, *9*, 1844.
[25] M. Cui, X. Wang, B. An, C. Zhang, X. Gui, K. Li, Y. Li, P. Ge, J. Zhang, C. Liu, C. Zhong, *Sci. Adv.* **2019**, *5*, eaax3155.
[26] W. J. Altenburg, N. A. Yewdall, D. F. M. Vervoort, M. H. M. E. Van Stevendaal, A. F. Mason, J. C. M. Van Hest, *Nat. Commun.* **2020**, *11*, 6282.
[27] E. W. Martin, T. Mittag, *Biochemistry* **2018**, *57*, 2478.
[28] C. W. Pak, M. Kosno, A. S. Holehouse, S. B. Padrick, A. Mittal, R. Ali, A. A. Yunus, D. R. Liu, R. V. Pappu, M. K. Rosen, *Mol. Cell* **2016**, *63*, 72.
[29] P. Mohanty, U. Kapoor, D. Sundaravadivelu Devarajan, T. M. Phan, A. Rizuan, J. Mittal, *Biochemistry* **2022**, *61*, 2443.
[30] T. S. Harmon, A. S. Holehouse, M. K. Rosen, R. V. Pappu, *eLife* **2017**, *6*, 30292.
[31] S. Kim, H. Y. Yoo, J. Huang, Y. Lee, S. Park, Y. Park, S. Jin, Y. M. Jung, H. Zeng, D. S. Hwang, Y. Jho, *ACS Nano* **2017**, *11*, 6764.
[32] O. Adame-Arana, C. A. Weber, V. Zaburdaev, J. Prost, F. Jülicher, *Biophys. J.* **2020**, *119*, 1590.
[33] J. A. Villegas, M. Heidenreich, E. D. Levy, *Nat. Chem. Biol.* **2022**, *18*, 1319.
[34] M. Dzuricky, B. A. Rogers, A. Shahid, P. S. Cremer, A. Chilkoti, *Nat. Chem.* **2020**, *12*, 814.
[35] L. Lemetti, A. Scacchi, Y. Yin, M. Shen, M. B. Linder, M. Sammalkorpi, A. S. Aranko, *Biomacromolecules* **2022**, *23*, 3142.
[36] S. F. Shimobayashi, P. Ronceray, D. W. Sanders, M. P. Haataja, C. P. Brangwynne, *Nature* **2021**, *599*, 503.
[37] M. Heidenreich, J. M. Georgeson, E. Locatelli, L. Rovigatti, S. K. Nandi, A. Steinberg, Y. Nadav, E. Shimoni, S. A. Safran, J. P. K. Doye, E. D. Levy, *Nat. Chem. Biol.* **2020**, *16*, 939.
[38] B. Gabryelczyk, F.-E. Sammalisto, J.-A. Gandier, J. Feng, G. Beaune, J. V. I. Timonen, M. B. Linder, *Mater. Today Bio* **2022**, *17*, 100492.
[39] A. D. Malay, T. Suzuki, T. Katashima, N. Kono, K. Arakawa, K. Numata, *Sci. Adv.* **2020**, *6*, eabb6030.
[40] J. M. Gosline, P. A. Guerette, C. S. Ortlepp, K. N. Savage, *J. Exp. Biol.* **1999**, *202*, 3295.
[41] J. Tormo, R. Lamed, A. J. Chirinol, E. Morag, E. A. Bayer, Y. Shoham, T. A. Steitz, *EMBO J.* **1996**, *15*, 5739.
[42] B. Zakeri, J. O. Fierer, E. Celik, E. C. Chittock, U. Schwarz-Linek, V. T. Moy, M. Howarth, *Proc. Natl. Acad. Sci. USA* **2012**, *109*.
[43] D. J. Leahy, I. Aukhil, H. P. Erickson, *Cell* **1996**, *84*, 155.
[44] A. Basak, O. Bateman, C. Slingsby, A. Pande, N. Asherie, O. Ogun, G. B. Benedek, J. Pande, *J. Mol. Biol.* **2003**, *328*, 1137.
[45] D. Fedorov, P. Batys, D. B. Hayes, M. Sammalkorpi, M. B. Linder, *Int. J. Biol. Macromol.* **2020**, *163*, 1995.
[46] P. Schuck, P. Rossmanith, *Biopolymers* **2000**, *54*, 328.
[47] Y. Shen, F. S. Ruggeri, D. Vigolo, A. Kamada, S. Qamar, A. Levin, C. Iserman, S. Alberti, P. S. George-Hyslop, T. P. J. Knowles, *Nat. Nanotechnol.* **2020**, *15*, 841.
[48] W. E. Arter, R. Qi, N. A. Erkamp, G. Krainer, K. Didi, T. J. Welsh, J. Acker, J. Nixon-Abell, S. Qamar, J. Guillén-Boixet, T. M. Franzmann, D. Kuster, A. A. Hyman, A. Borodavka, P. S. George-Hyslop, S. Alberti, T. P. J. Knowles, *Nat. Commun.* **2022**, *13*, 7845.
[49] L. Lemetti, S.-P. Hirvonen, D. Fedorov, P. Batys, M. Sammalkorpi, H. Tenhu, M. B. Linder, A. S. Aranko, *Eur. Polym. J.* **2019**, *112*, 539.
[50] J. J. Mcmanus, P. Charbonneau, E. Zaccarelli, N. Asherie, *Curr. Opin. Colloid Interface Sci.* **2016**, *22*, 73.
[51] J. Kuriyan, D. Eisenberg, *Nature* **2007**, *450*, 983.
[52] D. M. Mitrea, B. Chandra, M. C. Ferrolino, E. B. Gibbs, M. Tolbert, M. R. White, R. W. Kriwacki, *J. Mol. Biol.* **2018**, *430*, 4773.
[53] C. C. Miller, *Proc. R. Soc. Lond. Ser. Contain. Pap. Math. Phys. Character* **1997**, *106*, 724.
[54] S. Bucciarelli, J. S. Myung, B. Farago, S. Das, G. A. Vliegenthart, O. Holderer, R. G. Winkler, P. Schurtenberger, G. Gompper, A. Stradner, *Sci. Adv.* **2016**, *2*, e1601432.
[55] T. Hong, K. Iwashita, K. Shiraki, *Curr. Protein Pept. Sci.* **2018**, *19*, 746.
[56] A. M. Kusova, A. E. Sitnitsky, D. A. Faizullin, Y. F. Zuev, *J. Phys. Chem. A* **2019**, *123*, 10190.
[57] B. J. Dear, A. Chowdhury, J. J. Hung, C. A. Karouta, K. Ramachandran, M. P. Nieto, L. R. Wilks, A. Sharma, T. Y. Shay, J. K. Cheung, T. M. Truskett, K. P. Johnston, *Ind. Eng. Chem. Res.* **2019**, *58*, 22456.
[58] D. B. Hayes, *Practical Analytical Ultracentrifugation: What is biophysics?*, Vol. *1*, Principle Source Publisher, Monee IL, USA **2021**.
[59] E. W. Martin, F. E. Thomasen, N. M. Milkovic, M. J. Cuneo, C. R. Grace, A. Nourse, K. Lindorff-Larsen, T. Mittag, *Nucleic Acids Res.* **2021**, *49*, 2931.
[60] A. Stradner, H. Sedgwick, F. Cardinaux, W. C. K. Poon, S. U. Egelhaaf, P. Schurtenberger, *Nature* **2004**, *432*, 492.
[61] B. J. Borah, P. K. Maiti, C. Chakravarty, S. Yashonath, *J. Chem. Phys.* **2012**, *136*, 174510.
[62] J. D. Schmit, F. He, S. Mishra, R. R. Ketchem, C. E. Woods, B. A. Kerwin, *J. Phys. Chem. B* **2014**, *118*, 5044.
[63] S. Yadav, T. M. Laue, D. S. Kalonia, S. N. Singh, S. J. Shire, *Mol. Pharmaceutics* **2012**, *9*, 791.
[64] P. Schuck, *Biophys. J.* **2000**, *78*, 1606.
[65] B. Demeler, in *Anal. Ultracentrifugation Tech. Methods*, Royal Society Of Chemistry, Burlington House **2005**, pp. 210–229.
[66] J. Vistica, J. Dam, A. Balbo, E. Yikilmaz, R. A. Mariuzza, T. A. Rouault, P. Schuck, *Anal. Biochem.* **2004**, *326*, 234.
[67] C. A. Brautigam, in *Methods Enzymol*, (Ed: J. L. Cole), Academic Press, Cambridge, Massachusetts **2015**, pp. 109-133.
[68] J. Ellenberg, E. D. Siggia, J. E. Moreira, C. L. Smith, J. F. Presley, H. J. Worman, J. Lippincott-Schwartz, *J. Cell Biol.* **1997**, *138*, 1193.
[69] J. Sprakel, N. A. M. Besseling, M. A. Cohen Stuart, F. A. M. Leermakers, *Langmuir* **2008**, *24*, 1308.
[70] E. Spruijt, J. Sprakel, M. A. Cohen Stuart, J. Van Der Gucht, *Soft Matter* **2010**, *6*, 172.